Tanaka *et al. Earth, Planets and Space* (2017) 69:151
DOI 10.1186/s40623-017-0737-9

Earth, Planets and Space

FULL PAPER

Open Access

# Investigation of the fluid flow dynamic parameters for Newtonian and non-Newtonian materials: an approach to understanding the fluid flow-like structures within fault zones

H. Tanaka[1], Y. Shiomi[1,3] and K.-F. Ma[2*]

**Abstract**

To understand the fault zone fluid flow-like structure, namely the ductile deformation structure, often observed in the geological field (e.g., Ramsay and Huber The techniques of modern structure geology, vol. 1: strain analysis, Academia Press, London, 1983; Hobbs and Ord Structure geology: the mechanics of deforming metamorphic rocks, Vol. I: principles, Elsevier, Amsterdam, 2015), we applied a theoretical approach to estimate the rate of deformation, the shear stress and the time to form a streak-line pattern in the boundary layer of viscous fluids. We model the dynamics of streak lines in laminar boundary layers for Newtonian and pseudoplastic fluids and compare the results to those obtained via laboratory experiments. The structure of deformed streak lines obtained using our model is consistent with experimental observations, indicating that our model is appropriate for understanding the shear rate, flow time and shear stress based on the profile of deformed streak lines in the boundary layer in Newtonian and pseudoplastic viscous materials. This study improves our understanding of the transportation processes in fluids and of the transformation processes in fluid-like materials. Further application of this model could facilitate understanding the shear stress and time history of the fluid flow-like structure of fault zones observed in the field.

**Keywords:** Non-Newtonian material, Fluid flow, Dynamic parameters, Fault zone

## Introduction

Understanding the flow speed and direction in non-Newtonian fluids is important in many fields, such as for estimating the energy loss for airplanes and characterizing viscous-fluid flow within pipes. Several groups, particularly in the industrial community, have studied ductile deformation structure from fluid dynamics at the boundary layer near plates (Abdelhafez 1985; Hussaini et al. 1987; Ishak et al. 2007). Field investigations of the fault zones associated with ancient earthquakes (e.g., Additional file 1: Fig. S1 from Ramsay and Huber, 1983, and Additional file 1: Fig. S2 from Hobbs and Ord, 2015) exhibit similar ductile deformation features, but these features remain to be explained dynamically because most previous simulations of earthquake dynamics considered Newtonian materials. Recently, Ishak and Bachok (2009) extended fluid dynamics calculations to include non-Newtonian fluids, and similar studies were also performed by Zheng et al. (2008) and Dabrowski (2009). These studies estimated the dynamics of the fluid flow parameters. However, no thorough study has reconstructed the dynamics of fluid flow parameters based on geometric information, which is particularly important for the understanding of the ductile deformation structure within fault zones. These geological features observed in the field could extend from meters to kilometers in scale. This ductile, often asymmetric, deformation structure mainly made by viscous deformation of rock behaved as fluid flow. Because investigations of the fluid flow within and nearby fault zones are primarily performed via field surveys, observing the geometric information is a key to understanding the fluid flow dynamics.

*Correspondence: fong@ncu.edu.tw
[2] National Central University, Chung-Li, Taiwan
Full list of author information is available at the end of the article

Therefore, in this paper, we propose an inverse-calculation technique based on the geometry of the streak lines formed by fluid flow at the boundary layers of Newtonian and non-Newtonian fluids. Via this analysis, we obtain a better understanding of the time, flow rate and shear stress involved in the deformation of the streak lines at the boundary of infinite and semi-infinite plates. Estimation of the flow rate could be important to understand the evolution of the fault zone material, and the time and shear stress, thus, could help to quantify the process to understand the earthquake energy budget, or stress partition in a fault system. The proposed technique should be useful for estimating the fluid dynamics parameters based on the geometrical information of the ductile deformation structure.

To model nonlinear viscous fluids, we use the dimensionless velocity profile at the laminar boundary layer with a semi-infinite plate, as Ishak and Bachok (2009). Next, we calculate the dimensionless profiles of the deformed streak lines for fluid flows over infinite and semi-infinite plates and then estimate the time required for the streak lines to deform. Although the geological feature is more related to the "infinite plate" model, the "semi-infinite" model was used to reflect the further application from the semi-infinite model basis of Ishak and Bachok (2009), and the comparison made in the experiments in the later section, as that the ductile deformation structure could be correctly estimated from integrating the flow rate distribution. For geological indication, the "infinite" model could be comparable to the geological field observation of a long extension of the boundary (e.g., fault zone and fault line) to the ductile deformation structure in scale. The "semi-infinite" model could be comparable to the injection of the gouge from the main fault plain. From the profile of the deformed streak lines, we obtain the shear stress and shear rate at the boundary layer with infinite and semi-infinite plates. Initially, we derive the dimensionless profile of the deformed streak lines at the boundary layer by integrating the dimensionless velocity profile. Next, we compare the deformed dimensionless structure obtained from the calculation with the results of the flow experiments on Newtonian fluids performed by Nakayama (2011). Although Nakayama (2011) represented the motion of the flat plate to the stationary fluid, which is opposite to our model, the relative motion between the plate and fluid in both models is the same. We, thus, considered the experiment of Nakayama (2011) for our comparison.

## Estimation of the dynamic parameters

### Equations and models

To estimate the flow time, shear rate, and shear stress based on the geometry of the deformed streak lines at the laminar boundary layer of viscous fluids, we introduced the equations following Ishak and Bachok (2009).

For viscous materials, the relationship between the shear rate and the shear stress, $\tau$, over an infinite area is generally expressed as (Metzner and Reed 1955)

$$\tau = K\left(\frac{\partial u}{\partial y}\right)^n, \tag{1}$$

where $n$ is the power-law index, $u$ as the flow rate in $x$-component, and $K$ the viscosity. The fluid is Newtonian when $n = 1$, and when $n < 1$, the fluid is non-Newtonian for shear thinning. In this study, we consider the cases of Newtonian material of $n = 1$ and non-Newtonian of $n < 1$, as fault zone material is more considered as shear softening. For ductile shear zones as counterflow boundaries in pseudoplastic fluids by Talbot (1999), it considered the power-law fluid with different exponents $n$, which is exponent to the stress rather than to the strain of our Eq. (1), of 1.9–5. It is equivalent to our power-law index $n$, as the inverse to the exponent $n$, of ~ 0.2–0.53. Brodsky et al. (2009) studied a ductile texture in a series of asymmetrical intrusion structure suggested that non-Newtonian material can explain better the intrusion vein and the deformation of the ductile shear zone with $n = 1.5$ and $n = 5$, where $n$ is also as the power of shear stress proportional to the strain rate, and is inverse to our power-law index $n$. It is equivalent to our values of 0.2–0.67. Their result is also consistent with the study of Smith (1977), which suggested that non-Newtonian behavior is necessary and plays an important role in the formation of boudins and mullions observed in the field.

To understand the influence of non-Newtorian material in the fluid flow-like structure, in this model, we neglect the elastic, plastic and thermal properties of fluids and the heat generated by viscous friction first. The boundary layer in the fluid is assumed to be laminar, with a sufficiently small Reynolds number.

We consider the infinite plate model, where the fluid is initially stationary on an infinite plate. At a given point in time, fluid begins to move in a direction parallel to the plate surface at the fixed velocity $U_\infty$ (Fig. 1a) at far distance. As the fluid travels along the surface of the plate, the laminar boundary layer gradually becomes thicker. The fluid flow rate changed accordingly when it approaches the boundary. For the semi-infinite plate model, fluid flows at a fixed rate $U_\infty$ in the direction parallel to a stationary semi-infinite plate (Fig. 1b) at far distance. A boundary layer is generated when the fluid contacts the edge of the plate while the rate of fluid flow changed accordingly. The disturbance of the flow that occurs at the edge of a semi-infinite plate is ignored, and the laminar boundary layer is assumed to be stable. Geologically, the moving fluid might not be homogenous

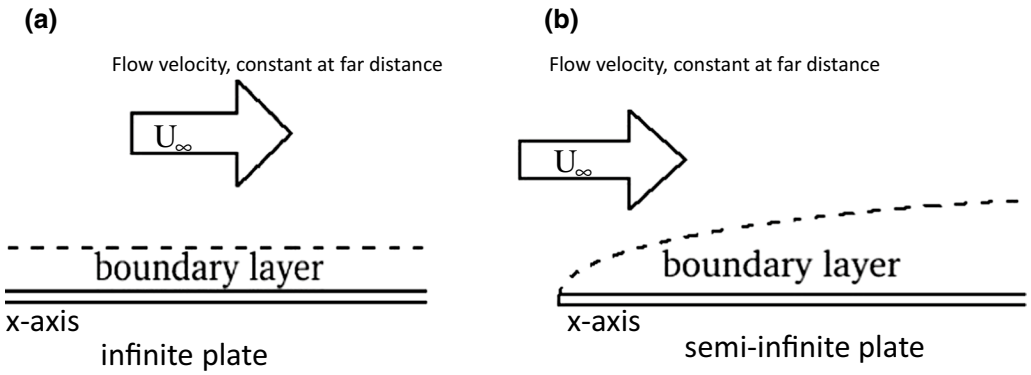


**Fig. 1** Illustrations of the two boundary layer models of two-dimensional laminar flow. Dashed lines separate the zero and nonzero domains of the velocity gradient of flow. **a** The infinite plate model, and **b** the semi-infinite plate model. The flat plate is fixed in *x*-direction, and fluid starts to flow parallel to the plate at a certain moment. $U_\infty$ denotes the flow velocity at far distance, which is parallel to the plate

over the space, and our model here represents the first order approximation to the geological structure.

Ishak and Bachok (2009) used Eq. (1) and the following equations to describe the dimensionless velocity profile of flow in a laminar boundary layer at a semi-infinite plate. The equations describing the boundary layer for $x$-component flow, $u$, and $y$-component flow, $v$, with density, $\rho$, are

$$\frac{\partial u}{\partial x} + \frac{\partial v}{\partial y} = 0 \tag{2}$$

$$u\frac{\partial u}{\partial x} + v\frac{\partial u}{\partial y} = \frac{1}{\rho}\frac{\partial \tau}{\partial y}. \tag{3}$$

The dimensionless distance in the $y$-direction, $\eta$, is

$$\eta = \left(\frac{Re}{x/L}\right)^{\left(\frac{1}{n+1}\right)}\frac{y}{L}, \tag{4}$$

where $Re$ is the Reynolds number and $L$ is the characteristic length. The dimensional stream function, $\psi$, is

$$\psi = LU_\infty\left(\frac{x/L}{Re}\right)^{\left(\frac{1}{n+1}\right)} f(\eta), \tag{5}$$

where $f(\eta)$ is the non-dimensional stream function, and $\psi$ satisfies

$$u = \frac{\partial \psi}{\partial y}, \quad v = -\frac{\partial \psi}{\partial x}. \tag{6}$$

The Reynolds number is given by

$$Re = \frac{\rho U_\infty^{2-n} L^n}{K}. \tag{7}$$

From these equations, Ishak and Bachok (2009) obtained

$$\left(|f''(\eta)|^{n-1} f''(\eta)\right)' + \frac{1}{n+1} f(\eta) f''(\eta) = 0. \tag{8}$$

We solved Eq. (8) by using the Runge–Kutta–Fehlberg method and the shooting technique, to obtain the velocity profile, $f'(\eta)$ as the $x$-component flow rate in $\eta$, as shown in Fig. 2. In comparable to the recent study of Deswita et al. (2010), our case is for impermeable and stationary plate with boundary conditions such as $f(0) = 0$,

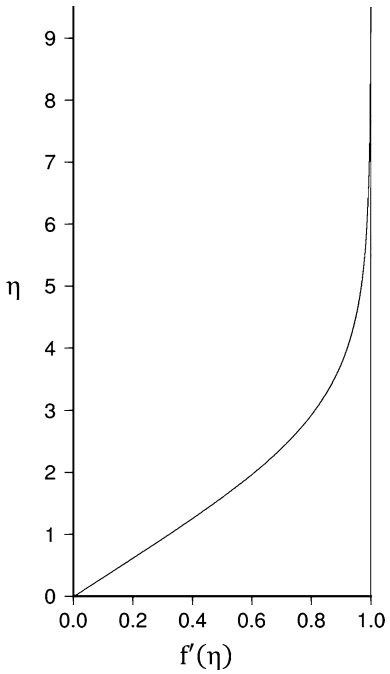


**Fig. 2** Flow rate, $f'(\eta)$, with distance, $\eta$, produced by the model of Ishak and Bachok (2009) for $n = 0.7$. $f'(\eta)$ is the $x$-component of the flow rate in $\eta$, and $\eta$ is the dimensionless distance perpendicular to the plate

$f'(0) = 0$, and $f'(\eta) \sim 1$ as $\eta \to \infty$. In the present calculation, the velocity $u(y)$ of the fluid at a distance $y$ from the plate is $U_\infty f'(\eta)$.

## Deformed streak lines in laminar flow

### *In the boundary layer of an infinite plate*

For the infinite plate model, the flow rate is constant along a line parallel to the $x$-axis. However, with time, the laminar boundary layer grows in the direction perpendicular to the plate. As the boundary layer grows, streak lines are deformed within the boundary layer.

Ishak and Bachok (2009) use Eqs. (4) and (5) to determine a dimensionless distance, $\eta$, in the $y$-direction. By combining these equations, we obtain

$$\eta = \left[\frac{\rho U_\infty^{(2-n)}}{xK}\right]^{\left(\frac{1}{n+1}\right)} y. \tag{9}$$

We substitute $x = U_\infty t$ into Eq. (9) to obtain

$$\eta = \left[\frac{\rho U_\infty^{(1-n)}}{tK}\right]^{\left(\frac{1}{n+1}\right)} y, \tag{10}$$

which leads to

$$\frac{y}{\eta} \propto t^{\left(\frac{1}{n+1}\right)}. \tag{11}$$

Equation (11) indicates that when the dimensionless distance perpendicular to the plate is $\eta_{t_1}$ at $t = t_1$, at $t_2 = at_1$, we have

$$\eta(t_2, y) = \left(\frac{t_2}{t_1}\right)^{-\left(\frac{1}{n+1}\right)} \eta(t_1, y), \tag{12}$$

where $t_2$ denotes the time that the displacement structure began to be generated, and with $x = U_\infty t_1$, and $X = U_\infty t_2$, we obtained

$$\eta(x, y)|_{t=t_1} = \left(\frac{x}{X}\right)^{-\left(\frac{1}{n+1}\right)} \eta_f, \tag{13}$$

where $\eta_f = \eta(X, y)|_{t=t_2}$. By applying $\eta$ to the dimensionless velocity profile shown in Fig. 2, as given by Ishak and Bachok (2009), we obtain the dimensionless flow rate $f'(\eta)$ for the infinite plate model.

To calculate the nonlinear profile of deformed streak lines, for each y, we calculate the corresponding values of $\eta(x, y)$ and $f'(\eta)$ for $x = 0$ to $X$ using an increment of $\Delta X$. Then, the results of the calculations are summed for each $y$. The results are divided by the total $f'(\eta)$ value, where $\eta$ is sufficiently large to be considered far from the plate in terms of the normalized values of $f'(\eta)$ over each y.

### *In the boundary layer of a semi-infinite plate*

A streak line is defined as a line drawn by connecting the points through which fluid particles flow at time t. Because of viscosity, the fluid velocity is lower in the boundary layer than in regions closer to the plate. This streak line becomes more deformed with time. The displacement of each fluid particle that is a certain distance from the plate at each moment is affected as soon as the particle passes over the tip of the plate or as soon as the fluid starts moving (Fig. 3a). In this case, to examine the spatial elements, we ignore the dynamics of the laminar boundary layer. We use Eq. (13) to determine $\eta$ at point $(x, y)$ in the fluid. By using $\eta$ in the distribution of the dimensionless velocity profile, $f(\eta)$, we obtain the $x$-component of the dimensionless flow velocity.

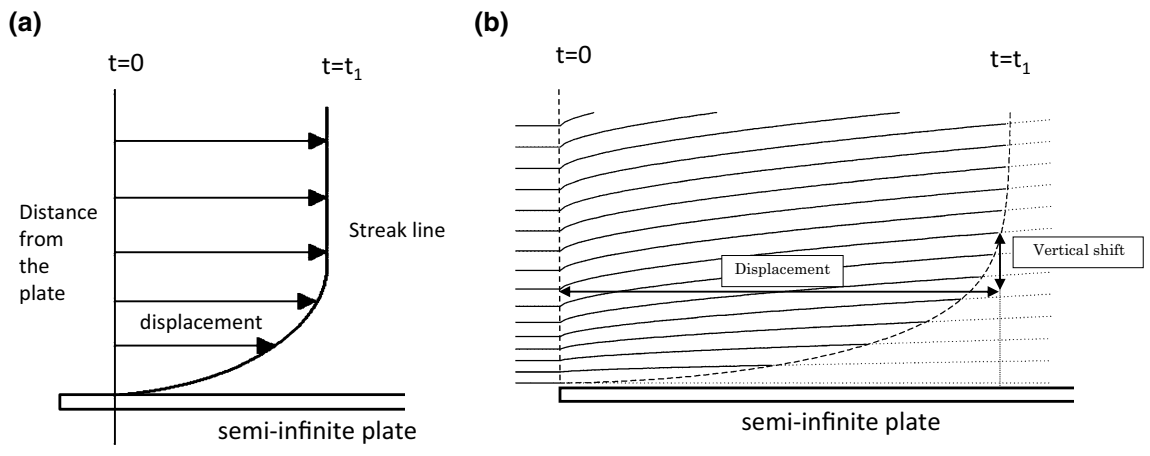


**Fig. 3** Illustrations of the "deformation structure" and "displacement structure." **a** The profile of a streak line. For each fluid particle, the distance from the plate and the displacement are calculated and plotted. **b** Non-dimensional displacement profile (dashed line) for a semi-infinite flat plate. Solid lines indicate the distance at which each fluid particle is distributed at a right angle to the apical portion of the plate over the defined time period. Dotted lines indicate the stream lines

Next, we calculate the streamline. The "vertical shift" is defined as the distance that the streamline shifts perpendicularly away from the semi-infinite plate (Fig. 3b) (Nakayama 2011). This shift also occurs inside the laminar boundary layer. Thus, streamlines can be expressed in terms of the parallel translation or "displacement" within the laminar boundary layer (Fig. 3b). To calculate a dimensionless streamline at a given distance from the plate, the distribution of the dimensionless vertical shift is required (Fig. 3b).

The vertical shift is determined as a function of $y$ in areas $S_1 = S_2$ in Fig. 4a (Nakayama 2011). This approach may also be applied to the dimensionless velocity profile of nonlinear fluids (Ishak and Bachok 2009). The distribution of the dimensionless vertical shift in a laminar boundary layer is calculated as follows: for $f(\eta = \eta_\infty) > 0.995$, which is regarded as sufficiently close to the dimensionless flow rate $f = 1$ at infinite distance, we determine the minimum $\eta$ at $f_\infty$ for $f(\eta = \eta_\infty) > 0.995$. In this case, the vertical shift $\eta^*(\eta)$ is almost identical to the displacement thickness for $\eta \geq \eta_\infty$.

Next, we estimate the vertical shift of the boundary layer. Considering the fluid as an aggregation of fluid particles, the vertical shift for each fluid particle is determined by the flow rate in the domain that is close to the plate, and the nonlinear vertical shift $\eta^*(\eta)$ from the plate is defined based on the points in areas A = B in Fig. 4b. The distribution of the vertical shift is then calculated using the recurrence technique. We consider the case $\eta = \eta_\infty - \Delta\eta$, which is infinitesimally close to the plate (separated by distance $\Delta y$). The displacement distance of a fluid particle is determined exclusively by the flow rate of the fluid particle at $\Delta y$. Thus, for $\eta_1 = \eta_\infty - \Delta\eta$, to balance the two areas B and A in Fig. 4b, the approximate equation becomes

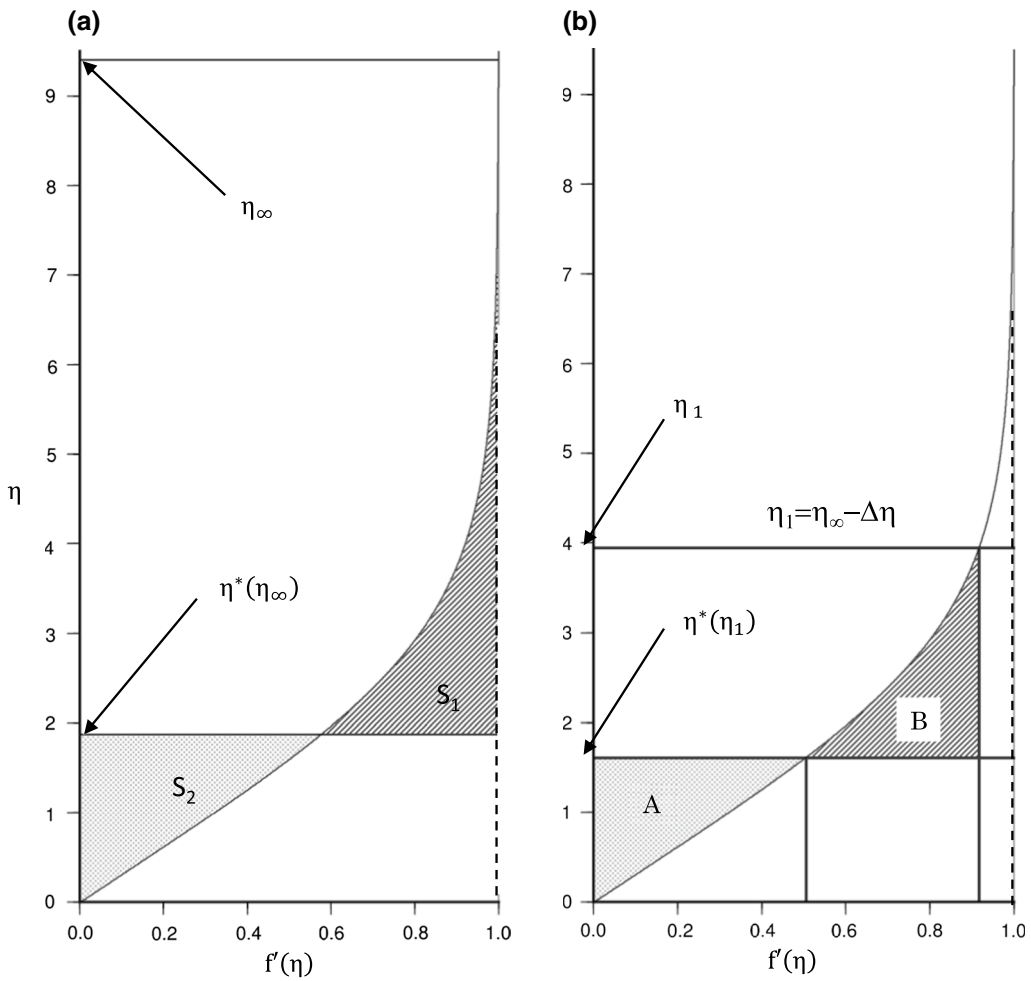


**Fig. 4** **a** Definition of the displacement thickness, $\eta^*(\eta_\infty)$, for the flow rate profile of the laminar boundary layer in areas $S_1 = S_2$. **b** Definition of the displacement distance, $\eta^*(\eta_1)$, for the flow rate profile of the laminar boundary layer for areas B = A at $\eta_1 = \eta_\infty - \Delta\eta$

$$\begin{aligned} \mathrm{B} &= S_1 - f'(\eta^*_\infty)\Delta\eta^* + \left\{f'(\eta^*_\infty) - f'(\eta^*_\infty - \Delta\eta^*)\right\}\frac{\Delta\eta^*}{2} \\ &\sim S_2 - \left\{f'(\eta^*_\infty) - f'(\eta^*_\infty - \Delta\eta^*)\right\}\frac{2\eta - \Delta\eta - 2\eta^*_\infty}{2} \\ &+ \left\{2f'(\eta_\infty - \Delta\eta) - f'(\eta^*_\infty) - f'(\eta^*_\infty - \Delta\eta^*)\right\}\frac{\Delta\eta^*}{2} = A, \end{aligned} \tag{14}$$

where $S_1 = S_2$ represents the slashed area of $\eta = \eta_\infty$, $\eta^*_\infty$ denotes $\eta^*$ at $\eta = \eta_\infty$, and $\Delta\eta^*$ is the deviation between $\eta^*_\infty$ and $\eta^*$ ($\eta_1 = \eta_\infty - \Delta\eta$). Thus, Eq. (14) can be rewritten as

$$\eta^*\big|_{\eta-\Delta\eta} \sim \frac{f'(\eta) - f'(\eta - \Delta\eta)}{f'(\eta - \Delta\eta)}\frac{2\eta - \Delta\eta - 2\eta^*}{2}, \tag{15}$$

for a generalized $\eta$. Considering the linear relationship between $f'(\eta)$ and $\eta$, we use the approximation $\eta^*(\eta) = \eta/2$ near the plate.

Next, we consider how to calculate the dimensionless streamline. In this calculation, we ignore any change in viscosity as a function of $y$ (perpendicular to the plate) that is attributable to the nonlinearity of the viscosity and the growth of the boundary layer over time.

Therefore, the displacement is determined only by the $x$-component of the flow rate in the boundary layer, and the growth of the vertical shift is proportional to the flow rate. Let $\eta^*(aX, y)$ represent the displacement distance as of a fluid particle in the direction perpendicular to the plate (i.e., the $y$-direction), where the dimensionless distance from the plate is $\eta_f$ at distance $x = aX$. Then, when $x = aX$, the dimensionless displacement distance $\eta^*(aX, \eta)$ becomes

$$\eta^*(aX, y) = a^{\frac{1}{n+1}}\eta^*(X, y). \tag{16}$$

Equation (16) describes the shape of the dimensionless streamlines. Using the dimensionless vertical shift $\eta^*(X, y)$, we find

$$\eta^*(x, \eta) = \left(1 - \frac{x}{X}\right)^{\left(\frac{1}{n+1}\right)}\eta^*(X, \eta). \tag{17}$$

As described above, the fluid flow is treated as a migration of fluid particles along dimensionless streamlines in the dimensionless profile of the flow rate. Thus, the distribution g ($\eta$) of the dimensionless displacement can also be determined. At $t = 0$, fluid particles are arranged parallel to the $y$-axis at $x = 0$ (original line) and then move because of their own velocity, deforming the original line. The initial conditions are $x = 0$ at $t = 0$. At $t = t_1$, the $x$ coordinate of a given fluid particle is $X$. Next, the movement of a fluid particle along the streamline passing along $\eta_f(t_1)$ at $x = X$ from $t = 0$ to $t = t_1$ could be calculated from $t = 0$ to $t_1$ using an interval of $\Delta t$. First, we consider position $(x, \eta)$ of a fluid particle and $f'(\eta)$. The dimensionless distance $\eta$ is calculated from Eq. (13) for the two models.

Because $\eta$ is determined, the corresponding $f'(\eta)$ is also determined. The $x$ coordinate of the next position is calculated by adding $f'(\eta)\Delta t$ to the previous $x$ coordinate. Because a fluid particle moves along the streamline, $y$, $\eta$ and $f'(\eta)$ at the next position can be determined accordingly. The calculation is repeated until $t = t_1$. Thus, $g(\eta)$, the non-dimensional displacement structure, is calculated from the $x/X$ ratio obtained from $t = 0$ to $t = t_1$ and $\eta_f$ is obtained using Eq. (17).

#### Calculation of flow time and shear stress

To calculate both the flow time and shear stress, we first use the displacement $x = X_f$ at $t = t_f$ and calculate the time required to generate a dimensionless deformed streak line. In the next section, this time is compared with the experimentally determined time to validate the model. Because $X_f = U_\infty t_f$, Eq. (9) becomes

$$\eta_f = \left[\frac{\rho X_f^{(1-n)}}{t_f^{2-n}K}\right]^{\left(\frac{1}{n+1}\right)} y, \tag{18}$$

for $x = X_f$. Thus, the time required to generate a deformed streak line is given by

$$t_f = \left[\left(\frac{y}{\eta_f}\right)^{(n+1)}\frac{\rho}{K}X_f^{(1-n)}\right]^{\left(\frac{1}{2-n}\right)}, \tag{19}$$

for both the infinite and semi-infinite models. Equation (19) shows that once the physical properties $(n, K, \rho)$, $\left(\frac{y}{\eta_f}\right)$ and $X_f$ of the fluid are known, the deformation time $t_f$ can be obtained, and thus, $U_\infty$ can be determined as $U_\infty = X_f/t_f$. However, Eq. (19) has a singularity at $n = 2$, where $t_f$ diverges. Similar results were reported by Denier and Dabrowski (2004) and Dabrowski (2009), suggesting infinite number of modal solutions for $n = 2$. Therefore, we believe that this issue remains unresolved. Based on these considerations, and as stated in the introduction, in this study we considered the case for $n \leq 1$, as we restrict the application of Eq. (19) to fluids with $n \leq 1$.

Next, we describe the calculation of the shear stress based on the profile of the deformed streak lines observed in the boundary layer in the fluid. In a boundary layer, the shear rate of fluid $f''(\eta)$ at $y = 0$ could be written as below with the observational displacement $\delta$ at $\eta_f$ from experiment,

$$\frac{\partial u}{\partial y}|_{y=0} = U_\infty \frac{\partial f^{'}(\eta)}{\partial \eta}\frac{\partial \eta}{\partial y}|_{y=0} = U_\infty f^{''}(\eta)\frac{\eta_f}{\delta}. \tag{20}$$

To evaluate the particle relationship between $y$ and $\eta$, which is necessary to estimate the time and stress during flow, in this study, we use "80% thickness" instead of "99% thickness," which is the general definition for the thickness of a boundary layer. This approach reduced both the measurement errors and the computation time. The relevant thickness is the vertical distance between the plate and the $y$-coordinate, where $x$ encompasses 80% of the displacement of the fluid particles at infinite distance $X_f$. The quantities $\eta_{\mathrm{sn}}$ for a semi-infinite plate (or $\eta_{\mathrm{in}}$ for an infinite plate) and $\delta$ can be obtained at 80% thickness from the dimensionless displacement-distribution graphs and the experimentally observed displacement structure. Thus, all the parameters in Eq. (19) can be obtained from either experimental results or models, allowing us to calculate the time to form deformed streak lines and the flow stress. $f''(\eta)$ at $y = 0$ can be obtained from the calculation of $f^{'}(\eta)$.

Thus, using $f''(\eta)$ at $y = 0$, which is estimated by the shooting technique, and Eqs. (1) and (20), we determine the total stress for the infinite plate model $\left(\eta_f = \eta_{\mathrm{in}}\right)$. The result is

$$\begin{aligned}\tau_{\mathrm{total}}(t) &= K\left[U_\infty f^{''}(\eta)\frac{\eta_{\mathrm{in}}}{\delta}\right]^n = K\left[U_\infty f^{''}(\eta)\left[\frac{\rho X_f^{(1-n)}K^{\frac{1}{n}}}{t^{(2-n)}}\right]^{\left(\frac{1}{1+n}\right)}\right]^n \\ &= \left[f^{''}(\eta)\left[\frac{\rho X_f^2 K^{\frac{1}{n}}}{t^3}\right]^{\frac{1}{1+n}}\right]^n = \left[f^{''}(\eta)\left[\frac{\rho U^3 K^{\frac{1}{n}}}{X_f}\right]^{\frac{1}{1+n}}\right]^n,\end{aligned} \tag{21}$$

where $U_\infty = X_f/t$ is the flow rate.

The result for the semi-infinite plate model $\left(y_f = y_{\mathrm{sn}}\right)$ is

$$\begin{aligned}\tau_{\mathrm{total}}(x) &= K\left[U_\infty f''(\eta)\frac{\eta_{\mathrm{sn}}}{\delta}\right]^n \\ &= K\left[U_\infty f''(\eta)\left\{\frac{\rho U_\infty^{(1-n)}}{tK}\right\}^{\left(\frac{1}{1+n}\right)}\right]^n \\ &= \left[f''(\eta)\left\{\frac{\rho U_\infty K^{\frac{1}{n}}}{x}\right\}^{\frac{1}{1+n}}\right]^n.\end{aligned} \tag{22}$$

The results of the calculations of the dimensionless displacement structure for the infinite and semi-infinite plate models using the equations derived above are shown in Fig. 5a and b, respectively. For any $n$, the graph is convex.

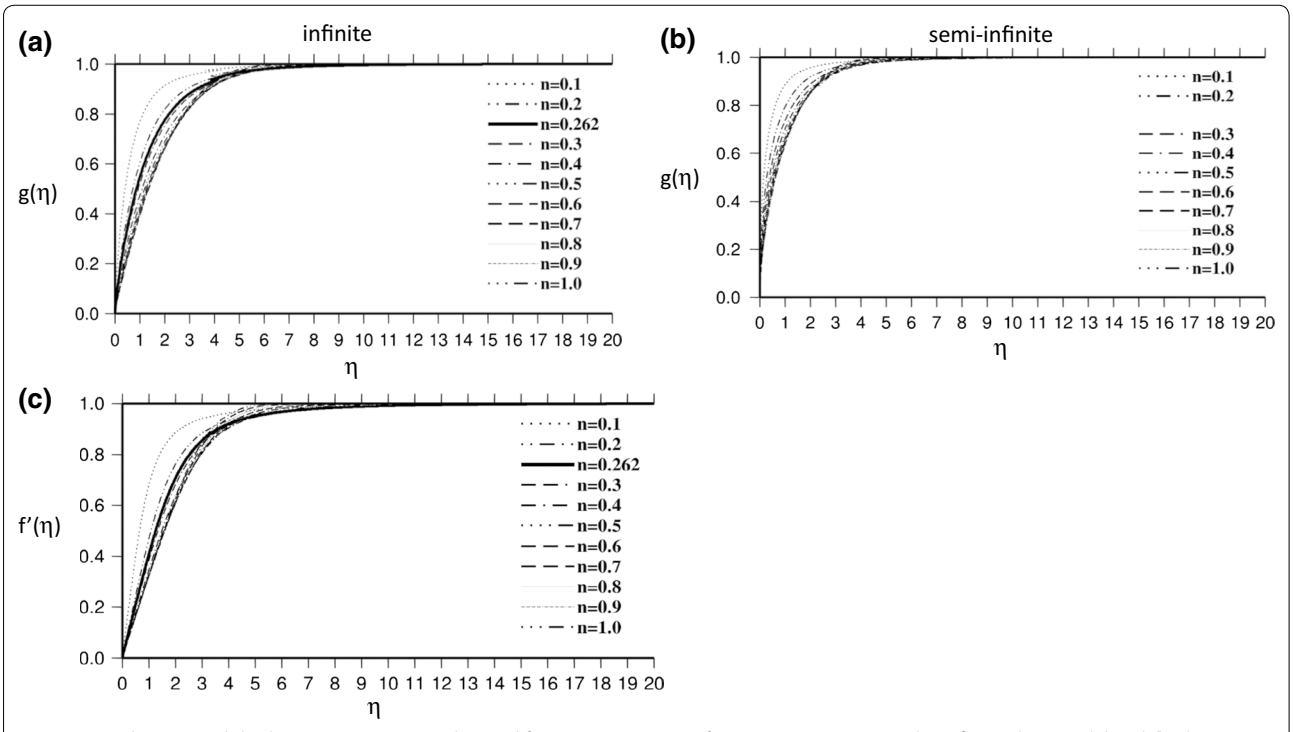


**Fig. 5** Non-dimensional displacement structures obtained for various $n$ ranging from 0.1 to 1.0 using (**a**) the infinite plate model and (**b**) the semi-infinite plate model. **c** The non-dimensional flow rate profiles of Ishak and Bachok (2009) for the infinite model. At approximately $n = 0.6$, the geometrical change of the non-dimensional flow rate structure graph is in agreement with the reduction in $n$. The graph is shifted down and right as $n$ decreases in the $n > 0.6$ domain, whereas it is shifted up and left as $n$ decreases in the $n < 0.6$ domain

For the results presented in Fig. 5a and b, the displacement structures for $n = 1.0$ have different curvatures than for other values of $n$. The velocity profile obtained by Ishak and Bachok (2009) shows similar characteristics, and Dabrowski (2009) reported similar results. However, the models of Zheng et al. (2008) do not exhibit these characteristics. The corresponding plots of $f'(\eta)$ for various $n$ of the infinite plate model are given in Fig. 5c and is further applied for the $f''(\eta)$ used in Eq. (21) to calculate the shear stress.

## Comparison to viscous-fluid experiments

The dynamic parameters of viscous fluid derived above are compared with the experimentally derived values. We consider two examples: The first example is water with $n = 1$, for which the experimental results were reported by Nakayama (2011). The second example is an edible sauce with $n < 1$, which is utilized to illustrate a pseudoplastic fluid. Because no existing examples reflect the deformed structure of the edible sauce, we use the density provided by the manufacturer and other parameters obtained by Miura et al. (2008) for this experiment.

### Newtonian fluid ($n = 1$): water

Water is a Newtonian fluid ($n = 1.0$) with a kinematic viscosity coefficient of $K/\rho = 1.002 \times 10^{-6}$ m$^2$/s and density of $\rho = 0.998$ g/cm$^3$ at 20 °C. We compare the result of the semi-infinite plate model with the experimental results reported by Nakayama (2011), in which the laminar boundary layer was visualized as shown in Fig. 6.

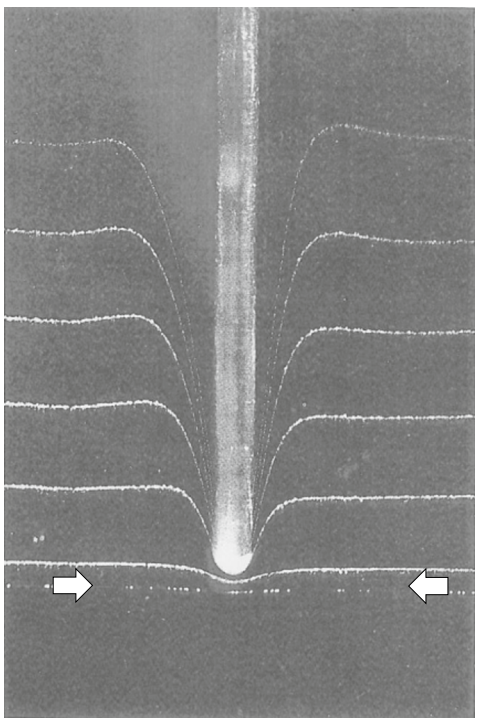


**Fig. 6** Photograph of the experiment performed to visualize the water boundary layer in water using the hydrogen bubble method (Nakayama 2011). The plate thickness was 5 mm, and the flow velocity was 0.6 cm/sec

In Fig. 6, the profile of the deformed streak lines can be clearly visualized as lines of hydrogen bubbles. In this case, the original streak lines are given by the direction of the wires that generate the hydrogen bubbles, which is perpendicular to the plate between the two arrows in Fig. 6. The flow rate in the experiment by Nakamura (2011) was $U_\infty = 6 \times 10^{-3}$ m/s. We estimated the flow rate from Fig. 6 based on its scale information: plate thickness = 5 mm, $X_f = 4.9 \times 10^{-2}$ m, $y = \delta = 5.6 \times 10^{-3}$ m and $\eta_{\mathrm{sn}} = 2.1$ for $n = 1$. Using these parameters, the deformation time is calculated to be $t_f = 7.1$ s and the flow rate $U_\infty = 6.9 \times 10^{-3}$ m/s based on equations of (19) and (22), respectively. The calculated flow rate is quite similar to the experimental value. Considering the $f''(\eta) = 0.332$ at $y = 0$ for $n = 1.0$ in Fig. 5c, we can obtained the shear stress $\tau$ from Eq. (22), which would have the values from approximately 1 to 0.1 Pa for a fluid particle moving from 1 mm to 1 cm, represented as an inverse linear relationship shown in Fig. 7a.

### Non-Newtonian fluid ($n < 1$): edible sauce ($n = 0.262$)

Taking the edible sauce with $n < 1$ as an example of a nonlinear fluid, the fluid parameters are $n = 0.262$ and $K = 142$ kg/$\left(\mathrm{m\ s}^{1.738}\right)$ at 20 °C (Miura et al. 2008) and $\rho = 1.19 \times 10^3$ kg/m$^3$ (provided by the manufacturer). Considering the case for infinite plate with $\eta_{\mathrm{in}} = 1.43$ and $n = 0.262$, according to Eq. (21), we could obtain the shear stress as function of time. Considering speed of fluid flow, we can also present the shear stress on the plate as a function of $X$ as shown in Fig. 7b for various flow rates of 0.2, 0.2, and 1 m/sec. Here, the plot was made using $f''(0) = 0.41$ for $n = 0.262$ according to Fig. 5c.

Through the distribution of the distance to the plate boundary for various flow rates, by the possible estimated flow rate examined in the field, it might give some indications on the shear stress distribution along the boundary of an identified fault for non-Newtonian material. In comparison with Fig. 7a of Newtonian material, the yielding shear stress from Non-Newtonian material is several order higher than the value of Newtonian material in our case of $n = 0.262$. For a certain distance, one-order difference in flow rate yields almost three-order difference in shear stress. And, the shear stresses drop significantly with distance, suggesting very large shear stress close to the plate boundary for non-Newtonian material. The estimation of the shear stress along the boundary using Newtonian material in simulation might give lower estimation of the shear stress.

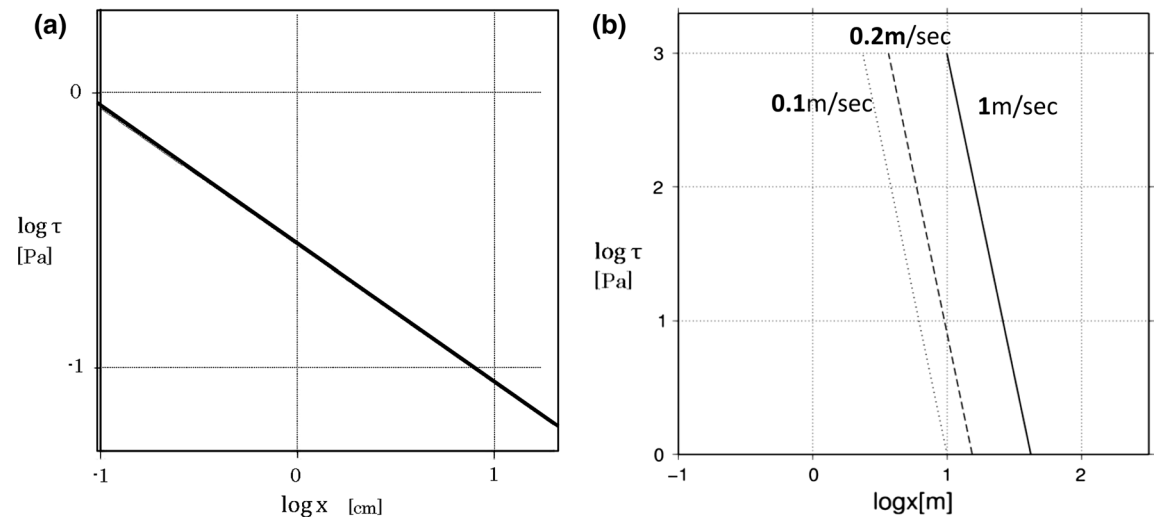


**Fig. 7** **a** Shear stress measured for the semi-infinite plate using water. "*x*" represents the distance from the tip of the flat plate in log–log scale. **b** Shear stress measured for the infinite plate using edible sauce. This figure shows how the shear stress changes as a fluid particle in the sauce moves "*x*" meters from its original point at flow rates of 0.1, 0.2, and 1 m/sec in the log–log scale

Comparing the calculated and experimental results, it reveals some technical errors in the estimation of the flow rate and time. One error might come from the difficulty in measuring the distance. Using the hydrogen bubble method, accurately measuring the distance from the tip of the plate in the direction parallel to the plate is difficult because bubbles crowd around the tip of the plate. Another possible error is the finite thickness of the plate because that the streamlines vary as a function of the plate thickness. Fortunately, these errors are not significant enough to compromise the validity of the calculation results.

For a flow with an extremely small Reynolds number, the viscosity of the fluid affects the dimensionless parameters, which renders the meaningless of Reynolds number (Leal 1992). Therefore, these models we derived here needed to be handled with care for the flows with extremely small Reynolds numbers (e.g., $n < 0.1$). Fortunately, most of the ductile deformation features were modeled considering with our equivalent power-law index $n$ greater than 0.1 (e.g., Talbot 1999; Brodsky et al. 2009).

## Summary

We derived a series of functions to estimate the time required for the generation of certain dynamic parameters (i.e., the flow rate, shear stress, and deformed structure) based on the geometric information of the boundary layer of the flow. The applications to two models: infinite plate and semi-infinite plate, were represented. For the semi-infinite plate model, a final displacement structure was obtained by computing the flow velocity at every spatial coordinate to obtain the resultant streamline, which is parallel to the plate in an infinite plate model. However, the dynamics of the laminar boundary layer in the direction perpendicular to the plate must be considered when it approaches the boundary. Therefore, the equations, thus, derived in this paper could be applied to estimate the flow velocity, stress and time required for the deformation of streamlines. And, the results could be further compared to the experimental observations. The calculated time required for the streamlines to deform and the flow velocity are consistent with the corresponding experimental results, suggesting the reliability of our derived equations and methodology applied in this paper. Because few experimental examples of the deformation structure in a nonlinear ($n < 1.0$) fluid exist, we used the parameters for edible sauce in our experiment. Although the presented results of our calculations are reasonable, we still suggest that the validity of the model might need to be justified with various fluids. This topic will be the subject of future experimental investigations. We hope it is possible to apply this technique to the observations in the field in the future although a comparable geological feature to the setting of this derived technique might remain some modifications. Once the ductile deformation structure could provide an indication of the relative displacement (e.g., vein across the deformation structure as a marker for displacement), it would be possible to estimate the time required for the formation of the ductile deformation structure and the equivalent ductile fluid flow speed as $U_{\infty}$, and, thus, the stress distribution along

the displacement. The flow direction as indication above could be considered as a flow parallel to the strongest deformed area. Our model setting is for an asymmetric shear deformation. For a larger scale, the crustal deformation observed by GPS data (Additional file 1: Fig. S3, http://mekira.gsi.go.jp/project/f3_10_5/ja/ondex.html) in Japan islands shows a significant asymmetric shear deformation feature, especially the motion across the right-lateral motion of Median Tectonic Line (MTL) in Shikoku island. It shows that not all of the right-lateral motions were resolved by MTL. Some shear motion remained to the north of MTL (northern regime of Shikoku island), which might be involved with possible viscous motion. The application of our derived technique might give some hints to the understanding of the large-scale asymmetric ductile deformation feature along MTL although more details might need to be addressed as compared to the GPS data through modeling. We hope the derived results in this study could facilitate better understanding on the fault zone dynamics, especially for viscous ductile deformation feature, which is often observed within and nearby fault zones in the field.

## Additional file

**Additional file 1.** Examples of photos of the fault zone fluid-like structure seen in the field and asymmetric ductile deformation structure.

### Authors' contributions

HT carried out the idea and basic theory in the modeling, and paper draft. YS developed the calculation, and paper draft. KM carried out the logical structure of paper, paper writing and submission. All authors read and approved the final manuscript.

### Author details

[1] University of Tokyo, Bunkyo, Tokyo 113-0033, Japan. [2] National Central University, Chung-Li, Taiwan. [3] Present Address: Circle Corrupt Inc., Tokyo, Japan.

### Acknowledgements

We sincerely thank Dr. Yasuki Nakayama of the Future Technology Research Institute and Professor Katsumi Aoyama of Tokai University for their comments regarding the details of the fluid-visualization experiment and for allowing us to include a photograph of their experiment in this paper. We also thank Dr. Takehiko Hiraga, Dr. Yasuko Takei and Dr. Atsuko Namiki for their helpful discussions regarding the formulation of fluid flow. Dr. Kuniyo Kawabata kindly helped with the equations. The help provided by Dr. Norio Shigematsu of the Advanced Industrial Science and Technology is also appreciated. Finally, we thank OTAFUKU SAUCE Co., Ltd., for providing the data regarding the edible sauce.

### Competing interests

The authors declare that they have no competing interests.

## Publisher's Note



Received: 9 May 2017 Accepted: 25 October 2017
Published online: 02 November 2017

### References

Abelhafez TA (1985) Skin friction and heat transfer on a continuous flat surface moving in a parallel free stream. Int J Heat Mass Transf 28:1234–1237
Brodsky EE, Rowe CD, Meneghini F, Moore JC (2009) A geological fingerprint of low-viscosity fault fluids mobilized during an earthquake. J Geophys Res 114:B01303. https://doi.org/10.1029/2008JB005633
Dabrowski PP (2009) Boundary layer flow in non-Newtonian fluids. PhD thesis, University of Aderaide (School of Mathematical Science)
Denier JP, Dabrowski PP (2004) On the boundary-layer equations for power-low fluids. Proc R Soc A 460:3143–3158
Deswita L, Ishak A, Nazar R (2010) Power-law fluid flow on a moving wall with suction and injection effects. Aust J Basic Appl Sci 4(8):2250–2256
Hobbs B, Ord A (2015) Structure geology: the mechanics of deforming metamorphic rocks, vol. I: principles. Elsevier, Amsterdam
Hussaini MY, Lakin WD, Nachman A (1987) On similarity solutions of a boundary layer problem with an upstream moving wall. SIAM J Appl Math 47:699–709
Ishak A, Bachok N (2009) Power-law fluid flow on a moving wall. Eur J Sci Res 34:55–60
Ishak A, Nazar R, Pop I (2007) The boundary-layer on a moving wall with suction and injection. Chin Phys Lett 24:2274–2276
Leal G (1992) Laminar flow and convective transport processes scaling principles and asymptotic analysis. Butterworth-Heinemann, Stoneham
Metzner AB, Reed JC (1955) Flow of non-newtonian fluids—correlation of the laminar, transition, and turbulent-flow regions. AIChE J 1:434–440
Miura Y, Hamasaki A, Nakagawa R, Takahashi K, Takano S, Nakano H (2008) Effect of temperature on rheological properties and flavor of sauces. Bull Hiroshima Jogakuin Univ 58:173–183
Nakayama Y (2011) Fluid dynamics new edition. Yokendo, Tokyo **(in Japanese)**
Ramsay JG, Huber MI (1983) The techniques of modern structure geology, vol. 1: strain analysis. Academia Press, London
Smith RB (1977) Formation of folds, boudinage, and mullions in non-Newtonian materials. Geol Soc Am Bull 88:312–320
Talbot CJ (1999) Ductile shear zones as counterflow boundaries in pseudoplastic fluids. J Struct Geol 21:1535–1551
Zheng L, Ting L, Zhang X (2008) Boundary layer flow on a moving surface in otherwise quiescent pseudo-plastic non-Newtonian fluids. J Univ Sci Technol 15:241–244